The Influence of a Vortex on a Freely Propagating Laminar Methane-Air Flame

Ki Yong Lee*

Andong National University, School of Mechanical Engineering, 388 Songchun-dong, Andong, Kyoungbuk 760-749, Korea

The change in the NO emission indices (EINO) in a two-dimensional plane has been investigated, which is due to the interaction between a vortex and methane-air flames established at different equivalence ratios, by solving the field equation. After solving the field equation, the spatial distribution of G-values is obtained. The NO emission index is calculated after applying the appropriate relation between the G-values and the NO production rate or the mass fraction of methane obtained from the library of freely propagating flames created from detailed simulations. When a vortex exists in a reacting flow field, in general EINO slightly increases, whereas EINO is lowered in the vicinity of the vortex regardless of flow direction. A change in vortex size has negligible impact on $EINO_T$ but increasing the vortex strength slightly increases $EINO_T$ in the domain of this study.

Key Words: Vortex, Equivalence, NO Emission Index, Field Equation, Flame Thickness

1. Introduction

The structure of a flame determines the distribution of heat release across a flame front. Pollutant processes, that are thermally dependent, can be slowed down if the heat release is manipulated so that it is dispersed over a larger than usual volume where the temperature level in the reaction zone is lowered. However, a dispersed flame zone may also allow for a larger region in which the super-equilibrium of key radical species occurs, thereby decreasing the relative chemical time associated with pollutant formation. Therefore, it is important to characterize the balance between flame zone thickening and pollutant formation.

One of the means to create a dispersed flame zone is to cause a flow disturbance by a vortex or through pulsation. Flow disturbances interact with flames in a complex manner through the coupling of the flow field with flame chemistry. For instance, if non-uniformities occur in the flow, these can contribute to flame extinction and enhanced preferential diffusion effects through stretch and curvature of the flame front.

A number of numerical studies have been devoted to the interactions of vortex structures and flames. Karasalo and Namer (1982) have studied a premixed laminar flame in a Karman vortex street. They have shown that the wrinkling of the flame depends strongly on the ratio of unburned to burned fluid densities as well as the vortex street frequency, the strength of the vortices, and the phase relations. The interaction of a vortex and a flame has been simulated by Marble (1985) to investigate the distortion of the surface of a non-premixed flame by a single viscous core vortex. It is shown that similarity for core radius growth and for the reactant consumption rate augmentation due to the vortex field is related to the Reynolds and Schmidt numbers. For a premixed flame, Peters and Williams (1988) investigated the roll-up of a flame surface by a

* **E-mail** : kylee@andong.ac.kr
TEL : +82-54-820-5899; **FAX** : +82-54-823-5495
Andong National University, School of Mechanical Engineering, 388 Songchun-dong, Andong, Kyoungbuk 760-749, Korea. (Manuscript **Received** July 25, 2003; **Revised** December 26, 2003)

single vortex using an asymptotic analysis for large Peclet numbers. In their work, relations for the growth of the reacted core, flame extinction by stretch for Lewis numbers greater than unity, and global influences of gas expansion associated with heat release are provided. Ashurst et al.(1988) investigated flame propagation in a constant density flame using the field equation and a pulsating flow field. They have shown that, in a steady frozen flow, the flame surface is composed of bulges connected by cusps, but in a pulsating flow, the appearance of flame cusps is damped. Ashurst and McMurtry (1989) investigated flame structure through vorticity distribution during premixed flame propagation in the velocity field of a single vortical region. They found that the monopole interacting with a premixed flame produces a vortex dipole structure through the baroclinic effect. Poinsot et al.(1990) studied the interaction of a laminar flame front with a vortex pair using direct numerical simulations. They were interested in flame quenching in a vortex from the perspective of viscous effects, stretch and curvature for small scales, and establishing a turbulent combustion diagram similar to that proposed by Borghi (1985). Rutland and Ferziger (1991) investigated the change in the vortex structure, vorticity distribution, and flame structure through the interaction of a vortex and a premixed flame. Using the full flame-vortex interaction, they determined that changing flame shape causes changes in the vortex structure, and that vorticity is produced by flame curvature. Rhee (2001) predicted flame cusping when a strong vortex pair interacted with the flame front from the simulation of a flame propagation using the Propagation of Surfaces under Curvature (PSC) algorithm.

For many applications the laminar flame thickness, which is determined by a reaction-diffusion process, is much smaller than the flow field length scales. Introducing the flamelet concept that allows partial decoupling of the reaction-diffusion process from the flow field, a relatively thin flame is considered in this study to solve only the propagation of its interface, i.e., for the flame front geometry. Therefore, the interaction of the interface propagation equation (also referred to as the field equation) is examined with the Navier-Stokes equations under different initial and boundary conditions. Using the results and a complete chemical library the change of the NO emission index is focussed in a two-dimensional plane for atmospheric methane-air flames established at different equivalence ratios.

2. Numerical Approach

The purpose of this study is to examine the change in the NO emission index due to the interaction between a vortex and a flame.

2.1 Governing equations and grid system

The simulation is limited to low Reynolds numbers leading to the assumption of low Mach number and performed with the governing equations including the equations of mass and momentum conservation, and state. The simulation is performed for constant temperature ($T=300$ K) and the change of the pressure in the calculation domain is generally negligible. Therefore, this simulation is for constant density flame propagation in a steady flow field.

To simulate flame propagation, it is convenient to adopt the field equation as an initial value problem (IVP) for a scalar field $G(x, t)$ whose level surfaces represent interfaces. The field equation derived with the surface assumed to be continuous and smooth is (Markstein, 1964):

$$\frac{\partial G}{\partial t}+u_i\frac{\partial G}{\partial x_i}=u_F|\nabla G| \tag{1}$$

where u_i is the flowfield velocity in the i direction, and u_F the flame propagation velocity normal to the interface.

When u_F is employed as a function of G, u_i, and their derivatives, Eq. (1) is valid (Kerstein et al., 1988). Shock discontinuities can develop in the solutions of initial value problems for Hamilton-Jacobi type equations such as Eq. (1), even for smooth initial data (Kerstein et al., 1988; Sethian, 1985). These discontinuities cause cusps which make the numerical simulation of the flame propagation problem difficult. By prod-

ucing Lipschitz continuous functions of G which satisfy an IVP, if the equation is understood in the almost everywhere sense, generalized solutions, which can overcome these features, can be defined, but are not unique (Crandall and Lions, 1984). However, it is known that the generalized solution, which corresponds to the flame propagation process considered here, can be obtained as the unique solution of the first order equation of Hamilton-Jacobi type, Eq. (1), if this equation is used with an added viscosity term on the righthand side (Crandall and Lions, 1984; Crandall and Lions, 1983). This solution is called as the viscosity solution.

This form of the field equation is employed to simulate constant density flame propagation in a premixed methane and air mixture,

$$\frac{\partial G}{\partial t}+u_i\frac{\partial G}{\partial x_i}=u_F\sqrt{\frac{\partial G}{\partial x_i}\frac{\partial G}{\partial x_i}}+\varepsilon\frac{\partial^2 G}{\partial x_i x_i} \quad (2)$$

where ε denotes viscosity. Eq. (2) is useful to achieve solutions which do not show spurious local maxima or minima, namely, solutions without cusps and pockets of unburned domain (Peters, 1984).

The calculation domain is discretized into a uniform spacing in rectangular coordinates that stay fixed with time. It consists of 0.02 m lengths in each of the x and y directions divided by 200 and 100 uniform spaces, respectively. The number of grids is 202×102 such that dx and dy are 0.0001 m and 0.0002 m, respectively, after the demonstration of grid independence with three cases, 102×102, 202×102, and 402×102 grid points, for $\phi=0.8$ flame.

2.2 Initial and boundary conditions

An Oseen vortex is chosen to interact with the flame. This vortex is one member of a family of vortex profiles that satisfies the Navier-Stokes equation (Panton, 1984). Its vorticity is described as

$$\omega_z=\frac{D}{\sigma^2}\exp\left(-\frac{r^2}{2\sigma^2}\right) \quad (3)$$

where $D\left(=\frac{\Gamma}{2\pi}\right)$ and $\sigma^2(=2\nu t)$ denote the initial vortex strength and size, respectively, and the constant Γ is a circulation pertaining the strength of the vortex, ν the kinematic viscosity, t the time, and r the radius.

The center of a counterclockwise vortex is positioned at $x=0.008$ m and $y=0.01$ m. The velocity induced by the vortex is constant at the boundary of the domain, and special boundary conditions are not required.

2.3 Initial flame structure

The initial flame structure is obtained from a detailed simulation of a freely propagating laminar methane-air flame using the SANDIA premixed flame code (Kee et al., 1989; Kee et al., 1985) at four different equivalence ratios $\phi=$ 0.7, 0.8, 1.0, and 1.2. The chemical mechanism consists of several hundred elementary reaction steps and involves 49 gas phase species, including nitrogen and argon which behave as inerts (Frenklach et al., 1994; Miller and Bowman, 1989). The spatial distribution of temperature so calculated is used as input for the initial values of the field equation.

Based on the flame structure of a free propagating flame, any flame characteristic or property P can be determined as a function of temperature or G, i.e., $P=P(T)=P(G)$, where P could refer to density, intercase propagation velocity normal to its contour, the mass fraction of methane, or the NO formation rate.

2.4 NO emission indices

The flame structure obtained from one dimensional laminar flame calculation can be expressed in terms of the mass production rate per unit flame surface of a given species (Takeno and Nishioka, 1993). The NO emission index (EINO) denotes the ratio of NO production to fuel consumption,

$$EINO=\frac{\int_x[W\dot{\omega}_{NO}dx]\times time}{\sum_i[\rho Y_{CH_4}]_{consumption}} \quad (4)$$

and the total NO emission index ($EINO_T$) is defined as

$$EINO_T = \frac{\int_y \int_x [W\dot{\omega}_{NO} dx dy] \times time}{\sum_{ij} [\rho Y_{CH_4}]_{consumption}} \quad (5)$$

where W denotes the molecular weight of NO, $\dot{\omega}_{NO}$ the NO production rate, ρ the density, Y_{CH_4} the mass fraction of CH_4, and i or j the x or y-wise direction, respectively. For sake of standardization, the time in Eq. (4) or (5) is taken to be that for a flame to propagate 0.01 m from its initial position. This time depends on the flame propagation velocity corresponding to different equivalence ratios.

After solving the field equation, the spatial distribution of G-values (or temperatures) is obtained. Applying the appropriate relation between the temperature and the NO production rate, or the mass fraction of CH_4 obtained from the library of freely propagating flames created from detailed simulations, the NO emission indices are calculated after applying Eqs. (4) and (5).

3. Results and Discussion

Let us examine the EINO along the y-wise direction in the absence of vorticity at a given time. This has a uniform profile along a line stretching from 0.004 m to 0.016 m. After subtracting the region (from 0.016−0.02 m) initially occupied by the flame, 160 grid points along the x-wise direction contain fresh mixture. Therefore, the initial region containing fresh mixture consists of 160×102 grid points in the x and the y-directions, respectively.

The NO emission index profiles are calculated for a variety of conditions for flames burning methane in air at different equivalence ratios. In Fig. 1, the EINO profiles are presented for different vortex sizes at a strength of D=0.0005 for a ϕ=0.8 flame. The solid line is the reference NO emission index $EINO_R$ in the absence of a vortex for an equivalent freely propagating flame. Even though the vortex sizes are altered, the EINO profiles are equivalent except around the vortex center. At the vortex center (x=0.008 m and y=0.01 m) the EINO values do not differ

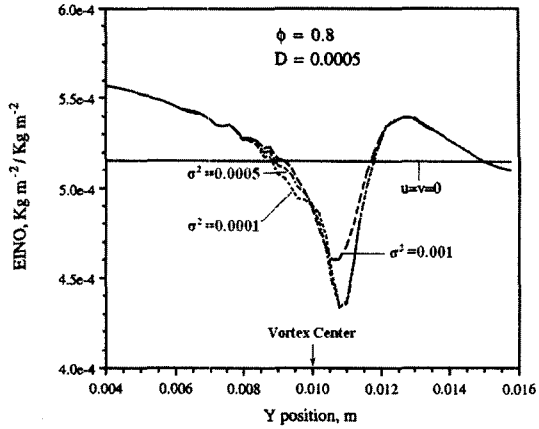

Fig. 1 The EINO profiles per area for different vortex sizes of constant strength D=0.0005 for a ϕ=0.8 flame

regardless of the magnitude of the vortex size, and are consistently lower than the $EINO_R$ that also corresponds to the condition u_q=0.

Below the vortex center (y<0.01 m, the direction of u_q is against the flame propagation), an increase in vortex size has little influence on the EINO, uniformly maintaining it lower than $EINO_R$. However, above the vortex center (y> 0.01 m, the direction of u_q is in the flame propagation), as the vortex size increases, the EINO profiles change, but are still lower than the reference value. The lowest EINO value occurs at y=0.011 m for σ^2=0.0005 and 0.001. At this point the velocities for the two cases have approximately the same values. Therefore, the lowest EINO value does not depend on the peak velocity in the flow field, but on the velocity at that specific spatial location.

3.1 Influence of interface shape and distribution

In Figs. 2 and 3, flame interface contours are presented, which are obtained from the simulations for two vortex sizes corresponding to a vortex of strength D=0.0005 for a ϕ=0.8 flame. The flames have propagated from the right side to the left side, and the G-values lie in the range from 300 K (at the left) to 1900 K (at the right). Upon comparing two figures, a small difference should be noted around the vortex center in the

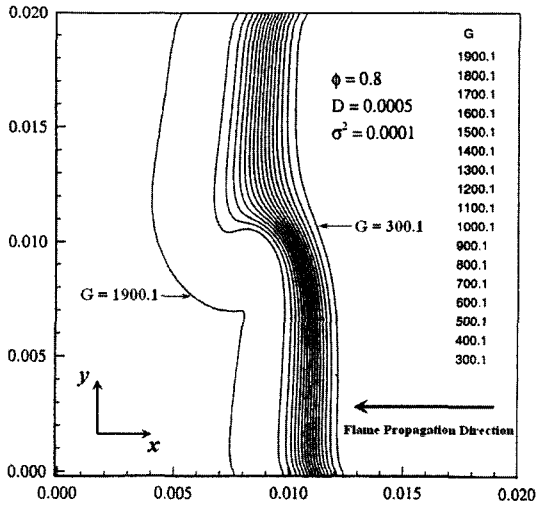

Fig. 2 Flame interface contours corresponding to a vortex of strength $D=0.0005$ and size $\sigma^2=0.0001$ for a $\phi=0.8$ flame

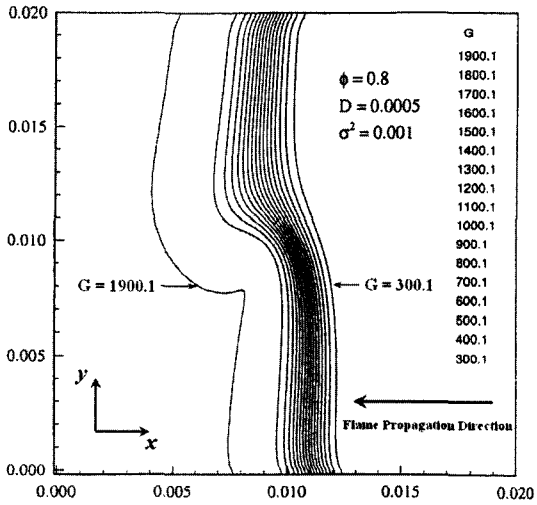

Fig. 3 Flame interface contours corresponding to a vortex of strength $D=0.0005$ and size $\sigma^2=0.001$ for a $\phi=0.8$ flame

flame shapes. Above the vortex center, the cusp of the flame shape of size $\sigma^2=0.0001$ coils slightly more than that of $\sigma^2=0.001$. This effect, which is manifest more at lower G-values, causes an increase in fuel consumption and a corresponding decrease in the EINO.

In the region $0.004\text{ m}<y<0.008\text{ m}$ below the vortex center where the flow direction is against that of flame propagation, higher G-value contours are curved towards the vortex center as y increases. There, the increase in fuel consumption is larger than that of NO production, and EINO values decrease with increasing y. These values are larger than the reference value, since the flow field hinders flame propagation, thereby decreasing the flame thickness which decreases the area available for fuel consumption.

In the region $0.012\text{ m}<y<0.016\text{ m}$ that lies above the vortex, the flow velocity occurs in the direction of flame propagation, and the thickness of the flame widens (in particular, note the wide separation between contours at $y=0.013$ m). The flame thickening increases the separation between consecutive temperature contours which allows for a larger spatial distribution around a temperature of 1700 K where the NO production rate peaks. It is also observed that just above the vortex center flame thickening effects are more manifest at higher temperatures. Therefore, in this region NO production increases faster than fuel consumption due to flame thickening at the higher temperatures, thus raising the EINO, since methane consumption is virtually negligible at temperatures of 1700 K and above. Proceeding upwards from $y=0.013$ m, the high temperature contours are separated by a virtually constant distance and curve in the clock wise direction. However, now the low temperature contours start to diverge so that fuel consumption increases although NO production is virtually constant. Therefore, the value of EINO rises above that of EINO_R immediately above the vortex center, and then decreases below it as y increases.

In Fig. 4, the EINO profiles per unit area are presented for different vortex strengths of constant size $\sigma^2=0.0001$ for a $\phi=0.8$ flame. The solid line corresponds to EINO_R, i.e., in the absence of a vortex in the flowfield. For the lower vortex strength $D=0.0001$ the EINO profile is close to the reference value, particularly at the vortex center, since a vortex of low strength does not significantly deform the flame shape as is shown in Fig. 5. As the vortex strength increases, the EINO profiles are lower than EINO_R in the

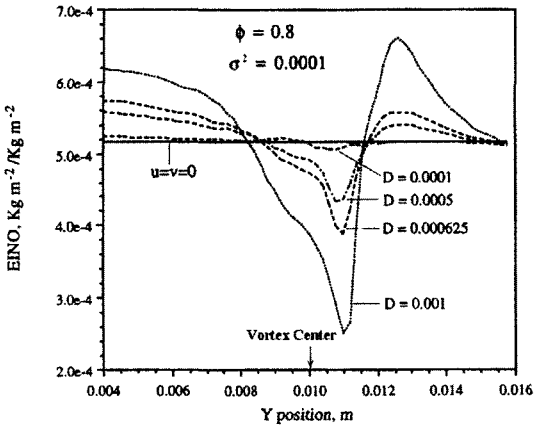

Fig. 4 The EINO profiles per area for different vortex strengths of constant size $\sigma^2=0.0001$ for a $\phi=0.8$ flame

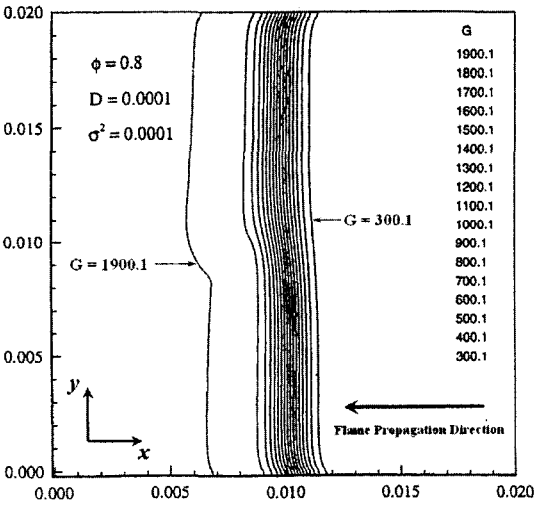

Fig. 5 Flame interface contours corresponding to a vortex of strength $D=0.0001$ and size $\sigma^2=0.0001$ for a $\phi=0.8$ flame

vicinity of the vortex, but are higher than $EINO_R$ away from it. The lowest EINO value occurs at $y\approx0.011$ m for the various vortex strengths.

In the immediate vicinity of the vortex 0.008 m$<y<$0.012 m the flow field is separated into two regions, one with flow velocities against the direction of flame propagation, and the other with flow in that direction. The EINO values lower than $EINO_R$ are due not to the direction of the flow, but to the increase in fuel consumption as shown in Fig. 6. Concurrently, the NO production does not significantly change in this region in accord with the arguments based on interface shape and separation made above.

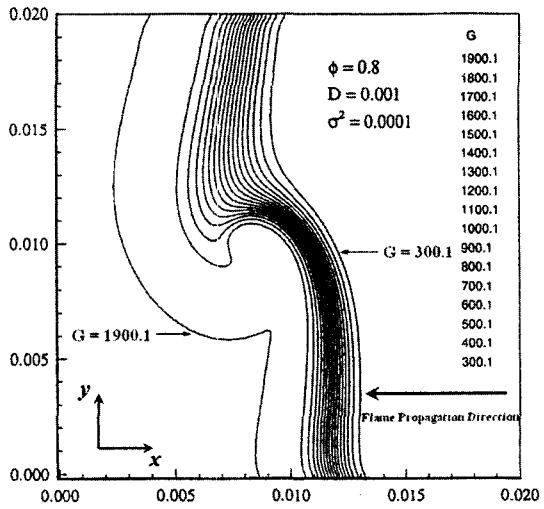

Fig. 6 Flame interface contours corresponding to a vortex of strength $D=0.001$ and size $\sigma^2=0.0001$ for a $\phi=0.8$ flame

3.2 Influence of flowfield

In regions removed from the vortex center, the EINO value appears to be related to the flow field direction. Where the flow is against the flame propagation direction, EINO values increase above $EINO_R$, since the flame thickness narrows, thereby decreasing fuel consumption over time, and causing the EINO to increase. Conversely, when the flow is in the direction of flame propagation, the width of the flame becomes larger, particularly at higher values of G. This causes an increase in the NO formation rate due to the increase in area occupied by high G-values. Fuel consumption also increases in the region between $y=0.012\sim0.013$ m, since flame thickening also occurs at relatively low G-values. However, the NO formation increase dominates, boosting the EINO value. Further upwards, at higher values of y, fuel consumption becomes dominant, since flame thickening is now biased towards lower G-values. Therefore, the EINO first increases and then decreases in that above the vortex as seen in Fig. 4.

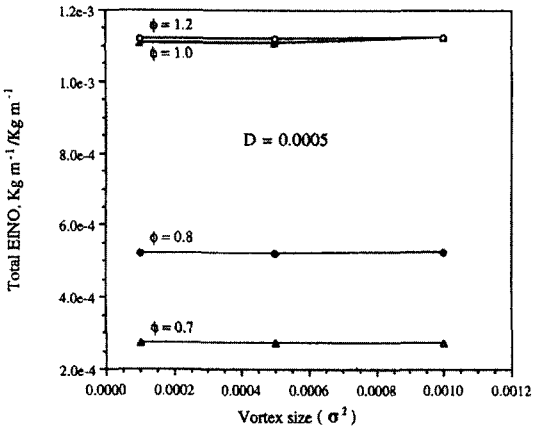

Fig. 7 The total EINO for different vortex sizes at a strength of $D=0.0005$ for flames corresponding to different equivalence ratios

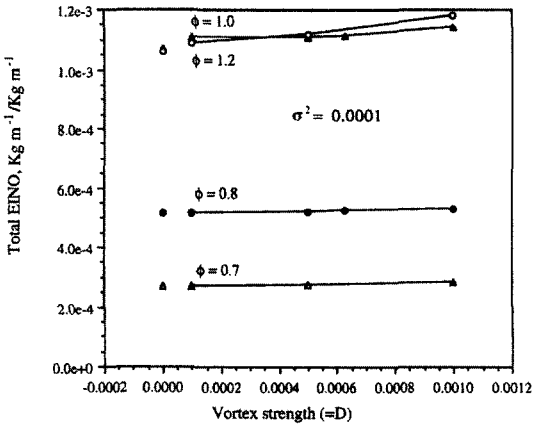

Fig. 8 The total EINO for different vortex strengths at a size of $\sigma^2=0.0001$ for flames corresponding to different equivalence ratios

The total EINO is calculated employing Eq. (5) for flames corresponding to different equivalence ratios. In Fig. 7, $EINO_T$ is presented for different vortex sizes for a vortex of strength $D=0.0005$. The change in $EINO_T$ with respect to vortex size is negligible for all the equivalence ratios considered. For the lean flames, the magnitudes of $EINO_T$ are proportional to the equivalence ratios, though this is not manifested for the rich flame, since $EINO_T$ is a function of the NO production as seen in Eq. (5). The NO production at $\phi=1.2$ has a similar distribution at high temperatures to that at $\phi=1.0$ for methane air flames. Figure 8 shows $EINO_T$ for different vortex strengths but of size $\sigma^2=0.0001$. As the vortex strength increases, $EINO_T$ values increase slightly for all ϕ in a manner similar to that for different vortex sizes.

4. Conclusions

By solving the field equation, the change in the NO emission index due to the interaction between a vortex and methane-air flames established at different equivalence ratios is investigated.

1. There are three distinct regions that influence the EINO.

(1) In the region where the flow occurs against the direction of flame propagation, increasing the velocity increases EINO due to a decrease in CH_4 consumption.

(2) In the vicinity of the vortex the EINO is lowered regardless of flow direction, since CH_4 consumption increases.

(3) Where the flow is in the direction of flame propagation, the EINO values reflect competition between an increase in both NO production and fuel consumption.

2. A change in vortex size has negligible impact on $EINO_T$.

3. Increasing the vortex strength slightly increases $EINO_T$ in the domain of this study.

References

Ashurst, W. M. and McMurtry, P. A., 1989, "Flame Generation of Vorticity : Vortex Dipoles from Monopoles," *Combust. Sci. and Tech.*, Vol. 66, pp. 17~37.

Ashurst, W. T., Sivashinsky, G. I. and Yakhot, V., 1988, "Flame Front Propagation in Non-steady Hydrodynamic Fields," *Combust. Sci. and Tech.*, Vol. 62, pp. 273~284.

Borghi, R., 1985, On the structure and morphology of turbulent premixed flames, *In Recent Advances in the Aerospace Sciences* (Edited by Casci, C.), Plenum Press, New York, pp. 117~138.

Crandall, M. G. and Lions, P. L., 1983, "Viscosity Solutions of Hamilton-Jacobi Equations,"

Trans. Amer. Math. Soc., Vol. 277, pp. 1~42.

Crandall, M. G. and Lions, P. L., 1984, "Two Approximations of Solutions of Hamilton-Jacobi Equations," Math. Comp., Vol. 43, pp. 1~19.

Frenklach, M., Wang, H., Bowman, C. T., Hanson, R. K., Smith, G. P., Golden, D. M., Gardiner, W. C. and Lissianski, V., 1994, "An Optimized Kinetics Model for Natural Gas Combustion," *Twenty-Fifth Symposium (International) on Combustion*, Irvine, California, Work-In-Progress Poster Session 3, Number 26.

Karasalo, I. and Namer, I., 1982, "Numerical Study of a Flame in a Karman Vortex Street," Combust. Flame, Vol. 47, pp. 255~267.

Kee, R. J., Grcar, J. F., Smooke, M. D., and Miller, J. A., 1985, "A Fortran Program for Modeling Steady Laminar One-Dimensional Premixed Flames," *Sandia Report*, SAND85-8240UC-401.

Kee, R. J., Rupley, F. M. and Miller, J. A., 1989, "Chemkin-II: A FORTRAN Chemical Kinetics Package for the Analysis of Gas Phase Chemical Kinetics," *Sandia Report*, SAND89-8009BUC-706.

Kerstein, A. R., Ashurst, W. T. and Williams, F. A., 1988, "Field Equation for Interface Propagation in an Unsteady Homogeneous flow Field," *Phys. Rev. A*, Vol. 17, pp. 2728~2731.

Marble, F. E., 1985, Growth of a Diffusion Flame in the Field of a Vortex, *In Recent Advances in the Aerospace Sciences* (Edited by Casci, C.), Plenum Press, New York, pp. 395~413.

Markstein, G. H., 1964, Theory of Flame Propagation, *In Nonsteady Flame Propagation* (Edited by Markstein, G. H.), The MaCMillan Company, New York.

Miller, J. A. and Bowman, C. T., 1989, "Mechanism and Modeling of Nitrogen Chemistry in Combustion," *Prog. Energy Combust. Sci.*, Vol. 15, pp. 287~338.

Panton, R. L., 1984, Incompressible Flow, John Wiley and Sons, New York.

Peters, N., 1984, "Laminar Diffusion Flamelet Models in Non-Premixed Turbulent Combustion," *Prog. Energy Combust. Sci.*, Vol. 10, pp. 319~339.

Peters, N. and Williams, F. A., 1988, "Premixed Combustion in a Vortex," *Twenty-Second Symposium (International) on Combustion*, The Combustion Institute, pp. 495~503.

Poinsot, T., Veynante, D. and Candel, S., 1990, "Diagrams of Premixed Turbulent Combustion Based on Direct Simulation," *Twenty-Third Symposium (International) on Combustion*, The Combustion Institute, pp. 613~619.

Rhee, C. W., 2001, "Flame Propagation, Flame-Vortex Interaction, Flame Cusping, Flameholding," *KSME International J.*, Vol. 15, pp. 623~629.

Rutland, C. J. and Ferziger, J. H., 1991, "Simulations of Flame-Vortex Interactions," *Combust. Flame*, Vol. 84, pp. 343~360.

Sethian, J. A., 1985, "Curvature and the Evolution of Fronts," *Commun. Math. Phys.*, Vol. 101, pp. 487~499.

Takeno, T. and Nishioka, M., 1993, "Species Conservation and Emission Indices for Flames Described by Similarity Solutions," *Combust. Flame*, Vol. 92, pp. 465~468.